^{13}C NMR Spin−Lattice Relaxation and Conformational Dynamics in a 1,4-Polybutadiene Melt

Grant D. Smith,* Oleg Borodin, and Dmitry Bedrov

Department of Materials Science and Engineering and Department of Chemical and Fuels Engineering, 122 South Central Campus Drive, Room 304, University of Utah, Salt Lake City, Utah 84112

Wolfgang Paul

Institut für Physik, Johannes Gutenberg Universität, Staudingerweg 7, D55099 Mainz, Germany

XiaoHua Qiu and M. D. Ediger

Department of Chemistry, University of Wisconsin−Madison, Madison, Wisconsin 53706

Received December 27, 2000

ABSTRACT: We have performed molecular dynamics (MD) simulations of a melt of 1,4-polybutadiene (PBD, 1622 Da) over the temperature range 400−273 K. ^{13}C NMR spin−lattice relaxation times (T_1) and nuclear Overhauser enhancement (NOE) values have been measured from 357 to 272 K for 12 different resonances. The T_1 and NOE values obtained from simulation C−H vector $P_2(t)$ orientational autocorrelation functions were in good agreement with experiment over the entire temperature range. Analysis of conformational dynamics from MD simulations revealed that T_1 depends much less strongly on the local chain microstructure than does the mean conformational transition time. Spin−lattice relaxation for a given nucleus could not be associated with the dynamics of any particular dihedral; instead, spin−lattice relaxation occurs as the result of multiple conformational events. However, a much closer correspondence was found between torsional autocorrelation times and the C−H vector $P_2(t)$ autocorrelation times upon which T_1 depends. Both processes exhibited stronger than exponential slowing with decreasing temperature. The non-Arrhenius temperature dependences of these relaxation times as well as the stretched-exponential character of the autocorrelation functions themselves were found to be consistent with increasing dynamic heterogeneity in conformational transition rates with decreasing temperature.

I. Introduction

Polybutadiene (PBD) has been the subject of extensive experimental investigation.[1] Much of this interest is engendered by the fact that PBD is a chemically simple polymer whose crystallization can be suppressed through random copolymerization of 1,4-trans, 1,4-cis, and 1,2-vinyl units, resulting in good glass-forming polymers. This copolymerization also allows for the systematic study of the influence of the chemical microstructure of the chain on melt and glass properties. Despite extensive experimental investigation, the relationship between macroscopic, segmental, and conformational dynamics in PBD, as well as their temperature dependence, remains poorly understood. Molecular dynamics (MD) simulations, in conjunction with experiment, have the potential to allow us to address these fundamental mechanistic questions, leading to a significantly improved understanding of polymer melt and glass dynamics.

In a previous paper,[2] we compared MD simulations and experimental measurements of local and chain dynamics in a melt of 1,4-polybutadiene. The (simulated) melt consisted of 40 random copolymer chains composed of 30 repeat units (1622 Da) with a 40% 1,4-cis/50% 1,4-trans/10% 1,2-vinyl microstructure, corresponding to the microstructure and molecular weight of the chains as synthesized. Simulations, ^{13}C NMR spin−lattice relaxation time (T_1), and nuclear Overhauser enhancement (NOE) measurements as well as neutron spin echo (NSE) measurements were performed on the PBD melt at 353 K. Excellent agreement with experiment was found for T_1 relaxation times and NOE values, indicating that the quantum chemistry based potential employed in the simulations yields an accurate description of local dynamics in PBD at 353 K. Similarly, good agreement with NSE measurements for the single chain intermediate coherent dynamic structure factor for 0.05 Å^{-1} ≤ q ≤ 0.30 Å^{-1} confirmed the ability of the simulations to reproduce chain dynamics on larger length scales at the temperature studied. Detailed analysis of the simulation trajectories and comparison of simulation, experiment and theory for polymer melt dynamics provided valuable insight into the mechanisms of chain motion in the PBD melt.[2−4] In addition, thermodynamic, static, and dynamic properties obtained from these simulations of the unentangled PBD melt have been used in conjunction with reptation theories in the accurate prediction of the linear viscoelastic properties of highly entangled PBD melts,[5] further demonstrating the accuracy of the simulations as well as the utility of studying the thermodynamic, static, and dynamic properties of unentangled polymers.

In this work, we have considerably extended the temperature range of both MD simulations and experimental ^{13}C NMR spin−lattice relaxation studies of the PBD melt. The goals of this study are to test the simulations through comparison of the temperature dependence of T_1 spin−lattice relaxation times and NOE

10.1021/ma002206q CCC: $20.00
Published on Web 06/12/2001

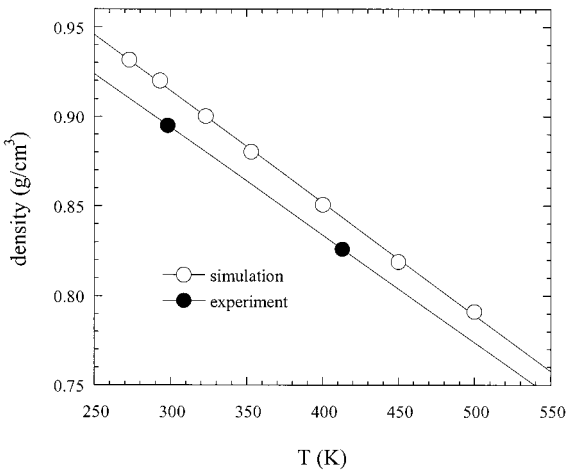

Figure 1. Density of the 1,4-polybutadiene melt as a function of temperature. Experimental data are from ref 7.

values with experiment and to gain a better understanding of the relationship between conformational dynamics and ^{13}C NMR spin−lattice relaxation in PBD melts. For this purpose, MD simulations have been performed over the temperature range 400−273 K while ^{13}C NMR T_1 and NOE measurements have been performed over the range 357−272 K.

II. Simulations and Experiments

The simulations were performed on the ensemble of 40 random PBD copolymers described briefly above and in detail in our previous work.[2] The quantum chemistry based united atom potential employed in the simulations is described in detail elsewhere.[6] Note that the quantum chemistry united atom potential does not include hydrogen atoms explicitly. For the purposes of determining static and dynamic properties that depend on hydrogen positions, we placed the atoms along the PBD chains based upon the stored united atom (carbon) positions using the procedure described previously.[2] Details of the simulation and experimental methodology can be found in our previous work.[2] For this study, the simulation trajectory at 353 K was extended from that reported previously[2] yielding a 40 ns total trajectory. The T_1 and NOE values reported here at 353 K are slightly different from those reported earlier due to improved statistics. The final melt configuration at 353 K was cooled to 323 K, and *NPT* dynamics were performed over 10 ns in order to obtain the equilibrium (1 atm) density. This was followed by 30 ns of *NVT* equilibration and 90 ns of *NVT* sampling. The procedure was repeated at 293 K with 50 ns of equilibration and 100 ns of sampling. For the 273 K system, 10 ns of *NPT* simulation were followed by 50 ns of *NVT* sampling; it is not feasible to simulate the PBD system for multiple Rouse times at this temperature as was done for higher temperatures. For 400 K, the 353 K system was heated to 400 K, where 10 ns of *NPT* simulation were followed by 20 ns of *NVT* sampling. Higher temperature simulations were also performed but were analyzed for density only. Figure 1 shows the density of the PBD melt from simulation as well as experimental data for a higher molecular weight PBD of similar microstructure.[7] Reasonable agreement can be seen. The thermal expansion coefficient of $\alpha = 7.1 \times 10^{-4}$ obtained at 353 K from simulation (assuming a linear dependence of density on temperature) is in excellent agreement with the value of 7.0×10^{-4} extracted from the experimental data.

The T_1 and NOE measurements that were performed on the PBD sample are described in detail in our previous work.[2] There only high-temperature results were reported. Here measurements covering the temperature range 357−272 K are reported. Uncertainties in the T_1 and NOE values are estimated at 2% and 5%, respectively. Uncertainties in NOE values involving vinyl group resonances are estimated at 10% due to poorer statistics.

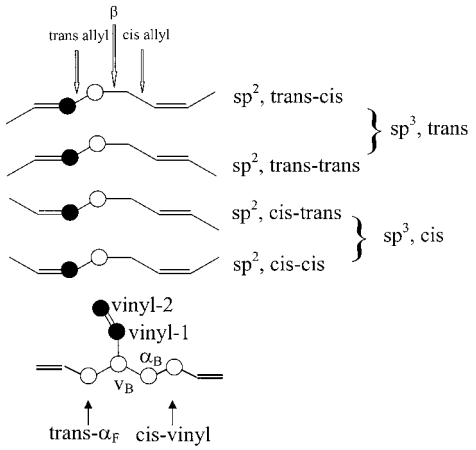

Figure 2. Chemical environments for experimentally resolvable ^{13}C NMR resonances. The sp^2 and sp^3 carbons are represented by filled and open circles, respectively. For example, the sp^2 carbon in a trans unit followed by a cis unit (resonance labeled trans−cis) can be differentiated from one followed by a trans unit (resonance labeled trans−trans), while the corresponding sp^3 resonances for the trans unit (resonance labeled trans) cannot be differentiated experimentally. The trans-α_F resonance involves an sp^3 carbon from a trans unit, while the *cis*-vinyl resonance involves an sp^3 carbon from a vinyl unit. Also labeled are the backbone dihedrals.

III. ^{13}C NMR T_1 Spin−Lattice Relaxation

We have determined the T_1 spin−lattice relaxation times and NOE values for the carbon nuclei associated with the 12 experimentally resolvable resonances illustrated in Figure 2. The experimentally measured T_1 and NOE values are related to the microscopic motion of the C−H vectors through the relationships[8]

$$\frac{1}{nT_1} = \mathrm{K}[J(\omega_\mathrm{H} - \omega_\mathrm{C}) + 3J(\omega_\mathrm{C}) + 6J(\omega_\mathrm{H} + \omega_\mathrm{C})] \quad (1)$$

$$\mathrm{NOE} = 1 + \frac{\gamma_\mathrm{H}}{\gamma_\mathrm{C}} \frac{6J(\omega_\mathrm{H} + \omega_\mathrm{C}) - J(\omega_\mathrm{H} - \omega_\mathrm{C})}{J(\omega_\mathrm{H} - \omega_\mathrm{C}) + 3J(\omega_\mathrm{C}) + 6J(\omega_\mathrm{H} + \omega_\mathrm{C})} \quad (2)$$

where n is the number of attached protons and ω_C and ω_H are the Larmor (angular) frequencies of the ^{13}C and ^{1}H nuclei, respectively, while γ_C and γ_H are the corresponding gyromagnetic ratios. The constant K is given by[8]

$$K = \frac{\hbar^2 {m_0}^2 {\gamma_\mathrm{H}}^2 {\gamma_\mathrm{C}}^2 \langle {r_\mathrm{CH}}^{-3} \rangle^2}{160\pi^2} \quad (3)$$

where m_0 is the permittivity of free space and r_CH is the carbon−hydrogen bond length. K assumes values of 2.29×10^9 and 2.42×10^9 s^{-2} for sp^3 and sp^2 nuclei, respectively.[8] The spectral density function $J(\omega)$ is given as[8]

$$J(\omega) = \frac{1}{2} \int_{-\infty}^{\infty} {P_2}^{\mathrm{CH}}(t) \mathrm{e}^{i\omega t}\, \mathrm{d}t \quad (4)$$

where

$${P_2}^{\mathrm{CH}}(\mathrm{i,t}) = \frac{1}{2}\{3\langle [\mathbf{e}_\mathrm{CH}(\mathrm{i,t}) \cdot \mathbf{e}_\mathrm{CH}(\mathrm{i,0})]^2 \rangle - 1\} \quad (5)$$

Here, $\mathbf{e}_\mathrm{CH}$ is a unit vector along a particular C−H bond, and the index i denotes differentiable resonances due

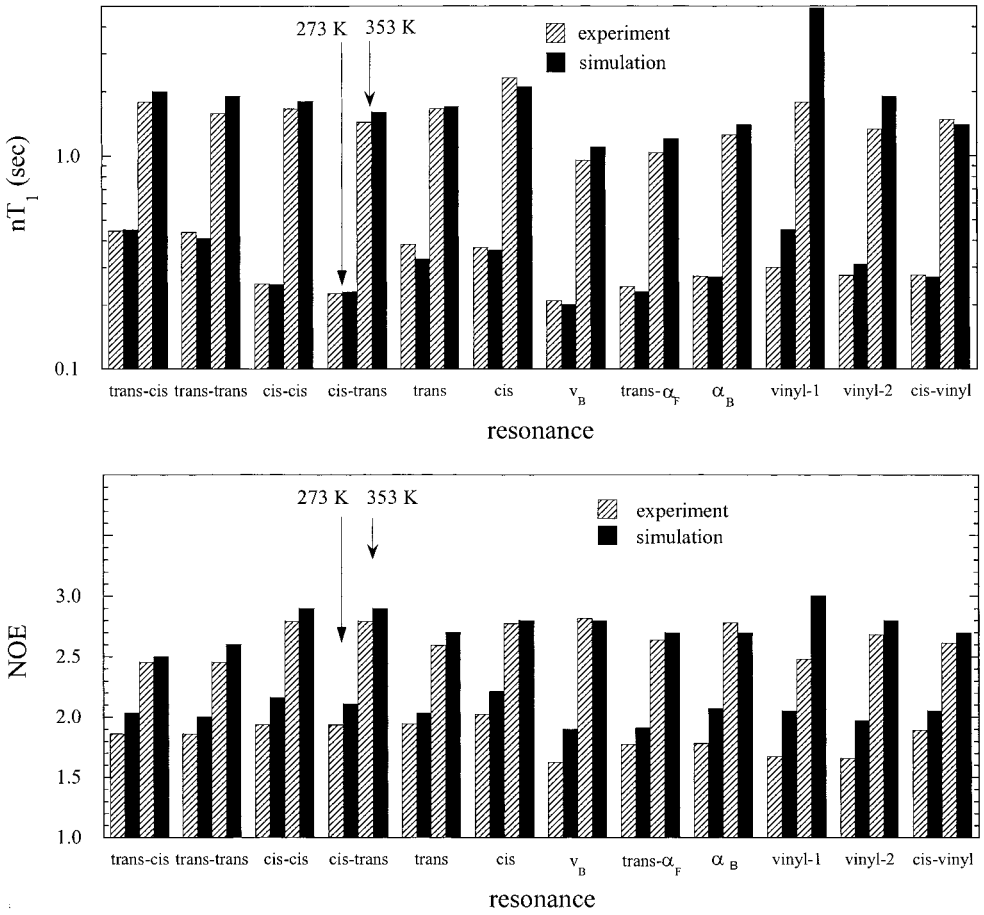

Figure 3. Spin-lattice relaxation times nT_1 (a) and NOE values (b) from experiment and simulation. Resonances are defined in Figure 2.

to local environment (see Figure 2). When the decay of the P_2^{CH} orientational autocorrelation function (OACF) is much faster than carbon and hydrogen resonances, extreme narrowing behavior is observed with

$$\frac{1}{nT_1} = 10K\tau_{CH} \tag{6}$$

where τ_{CH} is the P_2^{CH} autocorrelation time, given as the time integral of eq 5. In this regime, NOE = 3.

***P_2^{CH}* OACFs, *T_1*, and NOE Values.** The P_2^{CH} OACFs as determined from the simulation trajectories were found to be well represented at all temperatures by a stretched-exponential (Kohlrausch−Williams−Watts) plus a single-exponential function, as was found previously for the PBD melt at 353 K.[2] Representative P_2^{CH} OACFs with associated fits, as well as fitting parameters for P_2^{CH} OACFs for all experimentally distinguishable resonances at all simulation temperatures, are given in the appendix. The Fourier transforms of the fit-functions were utilized in evaluation of the spectral density (eq 4). The resulting T_1 and NOE values are compared with experiment in Figure 3, parts a and b, respectively, for the extreme temperatures of the experimental range, while T_1 and NOE values from simulation and experiment for all temperatures and resonances are tabulated in the appendix. A comparison of T_1 and NOE from experiment and simulation over the entire experimental temperature range is shown in Figure 4 for representative resonances. For T_1, excellent

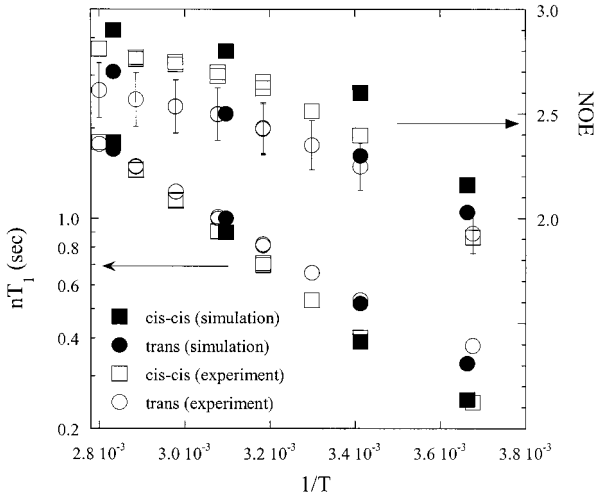

Figure 4. Spin lattice relaxation times nT_1 and NOE values for selected resonances from simulation and experiment as a function of temperature. Estimated experimental error bars for NOE (5%) are shown for one resonance. Estimated experimental error bars for nT_1 are smaller than the symbols.

agreement is seen between simulation and experiment for all resonances except those involving the two carbons in the vinyl group. As remarked in our previous paper,[2] too fast motion (too long T_1) of the vinyl group is consistent with the fact that the terminal CH_2 group in the vinyl group was represented using the same united atom potential as CH_2 used for the chain backbone. While necessary to give good conformational energies,

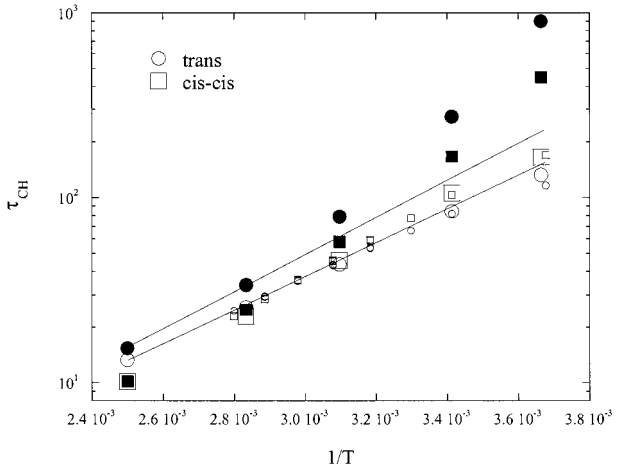

Figure 5. P_2^{CH} autocorrelation times τ_{CH} for selected resonances from eq 6 (large open symbols = simulation, small open symbols = experiment) and integrated OACFs (filled symbols). Solid lines demonstrate deviation of τ_{CH} from exponential temperature dependence (shown for the trans sp^3 resonance only).

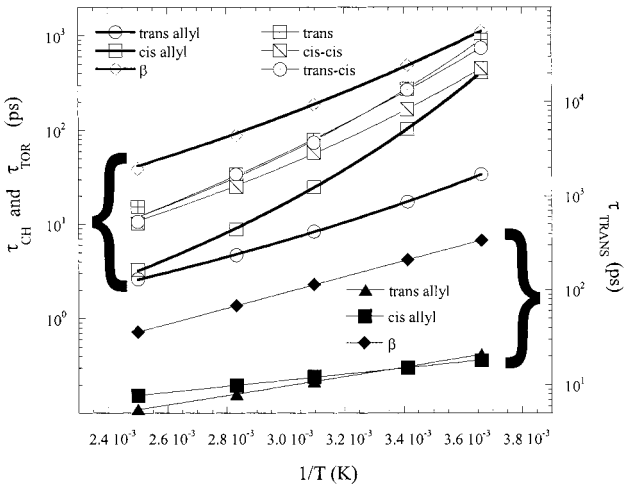

Figure 6. Mean conformational transition times τ_{TRANS} (filled symbols, thin lines), P_2^{CH} autocorrelation times τ_{CH} (opaque symbols, thick lines) and torsional autocorrelation times τ_{TOR} (open symbols, thin lines). Solid lines are exponential (mean conformational transition times) or Vogel−Fulcher (autocorrelation times) fits to the data.

this results in a terminal CH_2 which is actually too small, allowing too fast a rate of conformational transitions. For NOE, agreement with experiment is reasonable (excluding the vinyl group), and the temperature dependence of NOE is well represented. This level of agreement between experiment and simulation over a wide range of temperature, which to the best of our knowledge is far better than any previously reported, clearly demonstrates the value and utility of carefully parametrized quantum chemistry based polymer potentials.

Temperature Dependence of T_1 and P_2^{CH} Autocorrelation Times. The P_2^{CH} autocorrelation time τ_{CH} can be estimated from T_1 using eq 6. The resulting values are shown in Figure 5 as determined from both experiment and simulation T_1 values (eq 6) for the same resonances shown in Figure 4. Also shown in Figure 5 are the actual τ_{CH} values from simulation for these resonances, given by the time integral of eq 5. The τ_{CH} values determined from T_1 using eq 6 correspond to the actual autocorrelation times only in the limit of extreme narrowing. It can be seen in Figure 5 that the autocorrelation times from the OACFs and eq 6 merge at higher temperatures where faster dynamics lead to extreme narrowing behavior (see NOE values in the appendix). At higher temperatures T_1 (Figure 4) values show nearly exponential (Arrhenius) temperature dependence. At lower temperatures, weaker than exponential temperature dependence can be seen for T_1 while the temperature dependence of the autocorrelation time (from the integrated OACFs, Figure 6) increases with decreasing temperature. The latter effect represents a slowing of an identifiable microscopic dynamic quantity (decay of the C−H vector autocorrelation function) and is discussed in detail below. The temperature dependence of T_1 reflects that fact that T_1 is not simply related to microscopic dynamics outside of the extreme narrowing regime (see eq 4).

IV. Conformational Dynamics

Our previous simulations at 353 K revealed that the decay of the C−H vector OACF (eq 5) in PBD melts occurs primarily, but not entirely, as the result of local conformational transitions. This correspondence was established by the fact that conformational transition times and the P_2^{CH} autocorrelations times were within an order of magnitude of each other and that increasing rotational energy barriers for dihedrals by 0.4 kcal/mol had the same influence on conformational transition times and τ_{CH}; both were increased by a factor of 2. Here, we carry out a detailed analysis of conformational dynamics and their temperature dependence in PBD, and attempt to relate conformational dynamics to spin−lattice relaxation in PBD.

Figure 6 shows the mean conformational transition times τ_{TRANS} for the *trans*-allyl, *cis*-allyl, and β dihedrals (see Figure 2) as a function of temperature. A conformational transition is considered to have occurred when the state ($0° \le g^+ < 120°$, $120° \le t < 240°$, $240° \le g^- < 360°$, for β dihedrals, $-60° \le cis < 60°$, $60° \le s^+ < 180°$, $180° \le s^- < 300°$, for allyl dihedrals) of a dihedral differs at time $t + 1$ ps from that at time t. The allyl dihedrals exhibit faster dynamics than the alkyl dihedrals (β) at all temperatures. The τ_{TRANS} values are well represented by an Arrhenius temperature dependence. The apparent activation energies are 2.3, 1.3, and 3.8 kcal/mol for the *trans*-allyl, *cis*-allyl, and β dihedrals, respectively. From the conformational populations obtained from simulations, it is possible to calculate the relative conformational free energy

$$\Delta A_i(\phi) = -kT \ln P_i(\phi) \qquad (7)$$

where the index i denotes the dihedral type and $P_i(\phi)$ is the probability of dihedral angle ϕ relative to the most probable angle for that dihedral. The relative conformational free energies as shown in Figure 7 are nearly independent of temperature. These values closely resemble the intrinsic conformational potentials for the model compounds used in parametrization of the force field[2,6] indicating that condensed phase and chain connectivity effects do not strongly influence conformational populations in PBD. The activation energies for mean conformational transition times are consistent

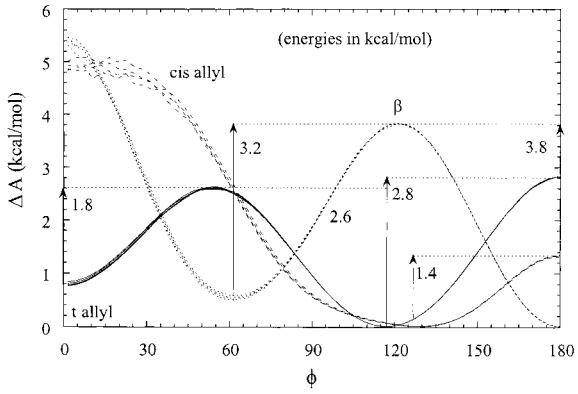

Figure 7. Relative conformational free energies for the principal backbone dihedrals in 1,4-polybutadiene. Values shown were determined from conformer populations at 273 K, 293, 323, and 353 K. Rotational free energy barriers are also indicated.

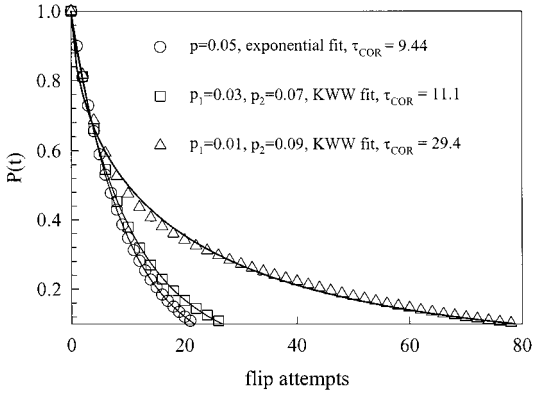

Figure 8. Autocorrelation function $P(t)$ for an uncorrelated two-state spin model. Lines are exponential (homogeneous dynamics) and stretched-exponential (heterogeneous dynamics) fits to the simulation data. Correlation times τ_{COR} for each set of flip rates are also given.

with the rotational free energy barriers shown in Figure 7, in each case closely matching the lowest barrier available to the lowest energy conformer.

V. Relationship between Conformational Dynamics and Spin−Lattice Relaxation in PBD

The decay of the C−H vector OACFs, and hence T_1, is related to conformational dynamics. However, the spin−lattice relaxation time cannot be simply related to the rate of conformational transitions. The dynamics of conformational transitions depend much more strongly on chemical environment than T_1. For example, in Figure 6, we see that conformational transition times vary by more than an order of magnitude at a given temperature. In contrast, Figure 3a shows that nT_1 values differ by no more than a factor of 2. It appears that spin−lattice relaxation occurs as the result of a multiple conformational events and that these events do not depend strongly upon the nuclei under consideration. When temperature effects are considered, it is difficult to establish any fundamental connection between conformational transitions and the C−H vector OACF upon which T_1 depends. For example, Figure 5 shows that τ_{CH} for the trans sp^3 carbon exhibits a non-Arrhenius temperature dependence and changes by almost 2 decades over the simulation temperature range. In contrast, Figure 6 shows that the mean transition times show Arrhenius temperature dependence and change by less than 1 decade over the same temperature range. Previous polymer simulations have also revealed differences between the temperature dependence of conformational transition times and C−H vector OACFs.[9]

A. Torsional Autocorrelation Function. To better understand the connection between conformational dynamics and spin−lattice relaxation we have investigated the torsional autocorrelation function (TACF) defined as

$$P(t) = \frac{\langle \cos \phi(t) \cos \phi(0) \rangle - \langle \cos \phi(0) \rangle^2}{\langle \cos \phi(0) \cos \phi(0) \rangle - \langle \cos \phi(0) \rangle^2} \qquad (8)$$

where $\phi(t)$ is the dihedral angle for given dihedral of a particular type and the ensemble average is over all dihedrals of that type. The torsional autocorrelation time τ_{TOR} is given as the time integral of eq 8, which was determined through KWW fits to the simulation $P(t)$ data. Figure 6 shows that τ_{TOR} exhibits non-Arrhenius behavior quite similar to that of the τ_{CH} with activation energies in the same range. Vogel−Fulcher fits of the form

$$\tau = A \exp[B/(T - T_o)] \qquad (9)$$

to the data shown yields average T_o values of 135 ± 25 K for both τ_{TOR} and τ_{CH}. This value is consistent with the glass transition temperature of 175 K obtained from rheological measurements on a PBD of similar microstructure.[10] The time scale of τ_{CH} for all primary (backbone) C−H vectors lies between the time scales of τ_{TOR} for the β dihedral and the allyl dihedrals over the entire temperature range investigated, indicating that decay of the P_2^{CH} OACFs likely occurs as a result of a combination of β and allyl transitions.

B. Dynamic Heterogeneity. To understand the connection between C−H vector dynamics and conformational dynamics, we must address the fact that while the mean conformational transition times exhibit Arrhenius temperature dependence over the entire range investigated, significantly greater slowing down is observed in τ_{CH} and τ_{TOR} with decreasing temperature (Figure 6). The mean conformational transition time measures the average waiting time for a dihedral and is sensitive to fast events—a few fast dihedrals with the remaining being quiescent will yield the same mean conformational transition time as a system in which all dihedrals show average dynamics. On the other hand, in order for the TACF to decay and, hence, at least for PBD, the P_2^{CH} OACF to decay, *each* dihedral must visit its available conformational states (e.g., g^+, g^-, t) with ensemble average probability. Hence, we can anticipate that unlike the mean conformation transition time, τ_{CH} and τ_{TOR} will be sensitive to the distribution of conformational transition rates—a broad distribution, with many dihedrals exhibiting much slower than average dynamics, can be expected to result in a much slower decaying TACF than a narrow distribution with the same mean conformational transition time. This is illustrated in Figure 8, which shows the autocorrelation function

$$P(t) = \langle s_i(t) s_i(0) \rangle \qquad (10)$$

for an ensemble of uncorrelated spins ($s_i = +1$ or -1). In each of the three cases illustrated, the mean prob-

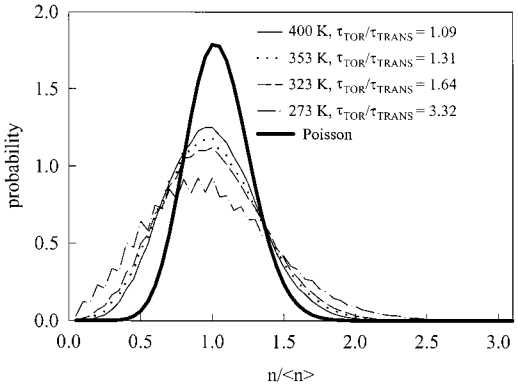

Figure 9. Distribution of the number of conformational transitions for β dihedrals after an average of 20 transitions, normalized by the average number of transitions (20). Also show is the ratio of the torsional autocorrelation time τ_{TOR} to the mean conformational transition time τ_{TRANS} for each temperature.

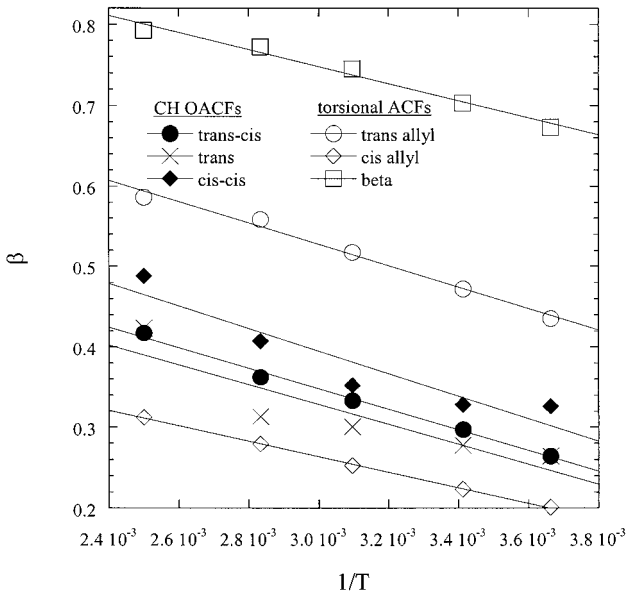

Figure 10. Stretching exponent β for MKWW fits to $P_2^{CH}(t)$ OACFs and KWW fits to torsional ACFs as a function of inverse temperature. Solid lines are linear fits that serve to guide the eye.

ability p that a given "dihedral" (spin) undergoes a "transition" (a spin flip via a Monte Carlo move) per unit time is constant at $p = {}^1/_{20}$. In the first case, each dihedral undergoes transitions with the mean probability (dynamically homogeneous), yielding single-exponential decay of ACF and a correlation time corresponding to the mean transition time. In the second and third cases, half of the dihedrals flip faster and half flip slower than the average, resulting in transition probabilities p_2 and p_1, respectively. As anticipated, the greater the dispersion in the transition rates, the longer the autocorrelation time. Also note that greater dispersion in the underlying transition rates leads to an autocorrelation function with a greater stretched-exponential character.

Figure 9 shows the distribution in the number of conformational transitions for the β dihedral in PBD after the average dihedral has undergone 20 transitions for various temperatures. The allyl dihedrals show analogous behavior. Also shown is the corresponding Poisson distribution that would be expected if conformational transitions were completely uncorrelated, i.e., if the system were dynamically homogeneous. Clearly the distribution of conformational transition rates becomes broader with decreasing temperature, indicating increasing conformational dynamic heterogeneity in the system. Figure 9 also shows τ_{TOR} for the β dihedrals in units of the mean conformational transition time for each temperature. In light of the simple spin model described above, the greater dynamic heterogeneity in conformational transition rates at lower temperatures is clearly consistent with the stronger temperature dependence of τ_{TOR} compared to the mean transition time, as well as the more stretched-exponential character of the autocorrelation function with decreasing temperature. The latter effect is illustrated in Figure 10, where the stretching exponent from fits to representative $P_2^{CH}(t)$ functions (see appendix) as well as KWW fits to the allyl and β TACF are shown as a function of temperature.

VI. Conclusions

A comparison of molecular dynamics simulations and ^{13}C NMR T_1 spin−lattice relaxation time and NOE measurements over a broad temperature range demonstrates remarkably good agreement for T_1 and NOE values. The temperature dependence of T_1 was found to correlate well with that of the P_2^{CH} autocorrelation time τ_{CH} at higher temperatures where NOE approaches 3 (extreme narrowing), as expected. However, neither T_1 nor τ_{CH} manifested temperature dependence in agreement with that observed for the mean conformational transition times, the fundamental time scale for the conformational events believed to lead to spin−lattice relaxation in PBD. While the conformational transition time showed Arrhenius temperature dependence over the entire range temperature range investigated, τ_{CH} showed stronger than exponential temperature dependence. Simulations reveal that τ_{CH} is closely related to torsional autocorrelation times τ_{TOR} for the β and allyl dihedrals. The non-Arrhenius temperature dependence of τ_{TOR} and τ_{CH} as well as the stretched-exponential character of their corresponding autocorrelation functions can be associated, at least in part, with dynamic heterogeneities in the rate of conformational transitions which increase with decreasing temperature.

Acknowledgment. G.D.S. gratefully acknowledges support of the Donors of the Petroleum Research Fund, administered by the American Chemical Society, through Awards G7-301 and SFB 262 for his stay in Mainz. M.D.E. and X.Q. are grateful for support from the National Science Foundation through DMR-9732483.

Appendix

Figure 11 shows representative $P_2^{CH}(t)$ OACFs with associated fits of the modified KWW (MKWW) function

$$P_2^{CH}(t) = A \exp[-(t/\tau)^{\beta}] + [1 - A] \exp[-t/t_o] \quad \text{(A1)}$$

Table 1 gives the MKWW fit parameters for the $P_2^{CH}(t)$

Table 1. Modified KWW Fitting Parameters for $P_2^{CH}(t)$ and Corresponding Correlation Times, nT_1, and NOE Values

temp (K)	value	trans-cis	trans−trans	cis−cis	cis−trans	trans	cis	ν_B	*trans*-α_F	α_B	vinyl-1	vinyl-2	*cis*-vinyl
273	A	0.984	1	0.714	0.675	0.857	0.815	0.688	0.727	0.787	0.852	0.775	0.785
	τ	34.0	49.8	65.2	72.9	54.9	26.6	148.2	156.3	119.1	5.4	25.4	83.6
	β	0.264	0.266	0.326	0.313	0.264	0.280	0.317	0.287	0.299	0.236	0.241	0.307
	t_0	9997	N/A	503	539	555	459	729	688	462	709	697	565
	τ_c	742	842	449	554	901	365	974	1480	979	261	747	671
	nT_1	0.45	0.41	0.25	0.23	0.33	0.36	0.20	0.23	0.27	0.45	0.31	0.27
	NOE	2.0	2.0	2.2	2.1	2.0	2.2	1.90	1.9	2.1	2.1	1.5	2.1
293	A	0.984	0.992	0.676	0.680	0.861	0.820	0.646	0.662	0.721	0.875	0.780	0.787
	τ	15.4	20.8	22.3	29.2	21.5	12.7	46.9	36.3	34.7	2.8	10.2	36.2
	β	0.297	0.299	0.328	0.324	0.277	0.266	0.305	0.275	0.249	0.261	0.257	0.297
	t_0	7461	19 605	214	215	156	148	274	263	195	278	270	215
	τ_c	267	344	166	202	274	200	356	429	295	81	221	322
	nT_1	0.64	0.58	0.39	0.36	0.52	0.58	0.29	0.32	0.38	0.78	0.46	0.39
	NOE	2.3	2.3	2.6	2.5	2.3	2.4	2.4	2.4	2.4	2.6	2.5	2.4
323	A	0.981	0.992	0.707	0.699	0.847	0.847	0.683	0.720	0.704	0.794	0.822	0.753
	τ	6.4	8.1	10.4	12.2	9.2	6.4	17.9	16.8	12.8	0.65	4.9	11.3
	β	0.333	0.329	0.352	0.353	0.300	0.303	0.346	0.315	0.310	0.423	0.289	0.306
	t_0	1923	3260	74	77	42	53	99	94	65	92	98	76
	τ_c	74	83	58	65	79	56	96	117	91	20	62	90
	nT_1	1.1	1.0	0.9	0.8	1.0	1.1	0.60	0.62	0.78	2.1	0.98	0.78
	NOE	2.1	2.5	2.8	2.8	2.5	2.6	2.7	2.6	2.6	2.9	2.7	2.6
353	A	0.981	0.989	0.786	0.770	0.827	0.897	0.716	0.687	0.703	0.821	0.893	0.741
	τ	3.3	3.9	6.6	7.6	4.9	4.1	10.4	8.4	7.6	0.52	3.6	6.7
	β	0.362	0.353	0.407	0.396	0.313	0.336	0.366	0.317	0.330	0.462	0.325	0.316
	t_0	1071	2109	37	34	13	20	38	33	25	42	43	26
	τ_c	34	41	25	28	34	23	43	53	41	9	26	43
	nT_1	2.0	1.9	1.8	1.6	1.7	2.1	1.1	1.2	1.4	4.9	1.9	1.4
400	A	0.963	0.972	1	1	0.984	1	1	1	1	0.816	1	1
	τ	1.4	1.8	4.8	5.4	3.2	2.6	7.4	6.5	5.5	0.32	2.4	4.4
	β	0.417	0.412	0.488	0.490	0.423	0.429	0.491	0.473	0.470	0.546	0.382	0.455
	t_0	177	218	N/A	N/A	394	N/A	N/A	N/A	N/A	14.9	N/A	N/A
	τ_c	10.7	11.4	10.2	11.3	15.4	7.2	16.3	14.4	12.5	3.2	9.0	10.5
	nT_1	4.1	3.9	4.1	3.7	3.3	6.1	2.7	3.1	3.5	13.0	5.0	4.2
	NOE	2.9	2.9	3.0	3.0	2.8	3.0	3.0	3.0	3.0	3.0	3.0	3.0

Table 2. Experimental nT_1 Values

	nT_1											
temp (K)	trans−cis	trans−trans	cis−cis	cis−trans	trans	cis	ν_B	*trans*-α_F	α_B	vinyl-1	vinyl-2	*cis*-vinyl
272	0.438	0.431	0.244	0.22	0.377	0.362	0.206	0.24	0.269	0.293	0.27	0.272
293	0.602	0.59	0.401	0.343	0.534	0.57	0.271	0.309	0.335	0.422	0.365	0.362
303.2	0.757	0.706	0.534	0.443	0.658	0.745	0.324	0.38	0.425	0.532	0.457	0.467
314.1	0.909	0.848	0.708	0.587	0.82	0.984	0.408	0.471	0.545	0.703	0.575	0.612
314.1	0.91	0.849	0.699	0.581	0.811	0.978	0.415	0.475	0.55	0.698	0.59	0.629
324.9	1.096	1.012	0.908	0.762	1.012	1.263	0.526	0.589	0.691	0.946	0.728	0.819
324.9	1.089	1.014	0.901	0.756	0.998	1.253	0.516	0.594	0.671	0.925	0.728	0.823
335.7	1.327	1.202	1.153	0.98	1.23	1.612	0.671	0.736	0.882	1.192	0.925	1.01
335.7	1.307	1.198	1.143	0.973	1.229	1.601	0.672	0.736	0.848	1.189	0.922	1.003
346.5	1.585	1.415	1.457	1.237	1.486	2.012	0.834	0.918	1.08	1.529	1.162	1.267
346.5	1.571	1.43	1.448	1.249	1.498	2.028	0.849	0.919	1.109	1.535	1.157	1.302
357.2	1.913	1.674	1.799	1.563	1.775	2.496	1.025	1.117	1.356	1.946	1.448	1.599

Table 3. Experimental NOE Values

	NOE											
temp (K)	trans−cis	trans−trans	cis−cis	cis−trans	trans	cis	ν_B	*trans*-α_F	α_B	vinyl-1	vinyl-2	*cis*-vinyl
272.0	1.848	1.848	1.91	1.91	1.928	2.003	1.601	1.756	1.764	1.653	1.636	1.873
293.0	2.059	2.059	2.398	2.398	2.248	2.420	2.075	2.08	2.11	2.071	2.114	2.191
303.2	2.132	2.132	2.512	2.512	2.351	2.551	2.317	2.29	2.388	2.237	2.193	2.305
314.1	2.208	2.208	2.621	2.621	2.432	2.631	2.505	2.375	2.571	2.389	2.462	2.582
314.1	2.266	2.266	2.654	2.654	2.426	2.634	2.539	2.377	2.619	2.395	2.362	2.465
324.9	2.284	2.284	2.698	2.698	2.497	2.700	2.644	2.481	2.687	2.451	2.556	2.428
324.9	2.338	2.338	2.68	2.68	2.499	2.704	2.555	2.511	2.765	2.492	2.427	2.796
335.7	2.392	2.392	2.736	2.736	2.536	2.732	2.504	2.521	2.672	2.526	2.62	2.606
335.7	2.342	2.342	2.747	2.747	2.534	2.734	2.709	2.642	2.718	2.482	2.585	2.838
346.5	2.428	2.428	2.77	2.77	2.568	2.759	2.676	2.537	2.744	2.484	2.67	2.569
346.5	2.379	2.379	2.761	2.761	2.568	2.753	2.792	2.693	2.862	2.486	2.634	2.654
357.2	2.487	2.487	2.809	2.809	2.612	2.784	2.869	2.655	2.765	2.479	2.708	2.617

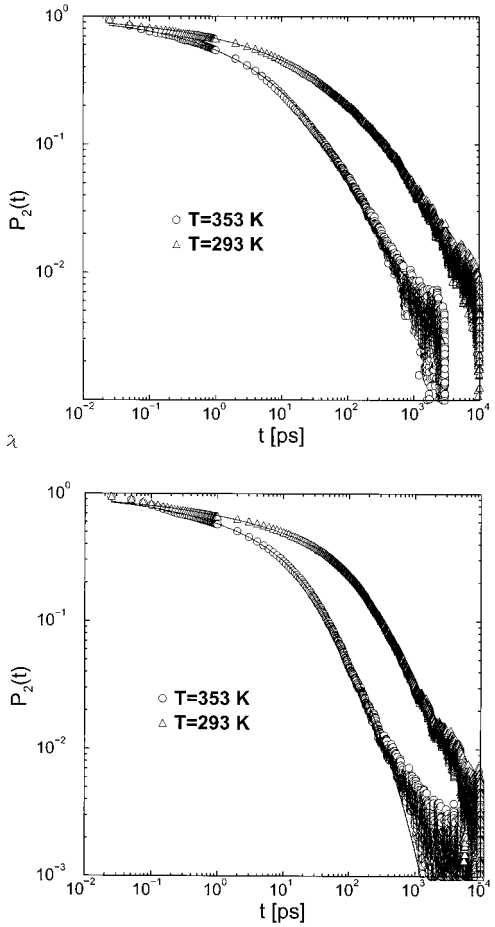

Figure 11. $P_2^{CH}(t)$ and MKWW fits for representative C−H vectors: (a) trans−trans and (b) cis.

for each experimentally resolved resonance along with autocorrelation times, nT_1 and NOE values for PBD determined from the fit function through application of eqs 1−5. Table 2 gives the experimentally determined nT_1 values while Table 3 gives the experimentally determined NOE values for PBD as a function of temperature.

References and Notes

(1) See for example Frick, B.; Richter, D. *Science* **1995**, *267*, 1939.

(2) Smith, G. D.; Paul, W.; Monkenbusch, M.; Willner, L.; Richter, D.; Qiu, X. H.; Ediger, M. D. *Macromolecules* **1999**, *32*, 8857.

(3) Smith, G. D.; Paul, W.; Monkenbusch, M.; Richter, D. *Chem. Phys.* **2000**, *261*, 61.

(4) Smith, G. D.; Paul, W.; Monkenbusch, M.; Richter, D. *J. Chem. Phys.*, in press.

(5) Byutner, O.; Smith, G. D. *Macromolecules* **2001**, *34*, 134.

(6) Smith, G. D.; Paul, W. *J. Phys. Chem.* **1998**, *102*, 1200.

(7) Fetter, L. J.; Lohse, D. J.; Richter, D.; Witten, T. A.; Zirkel. A. *Macromolecules* **1994**, *27*, 4639.

(8) Gisser, D. J.; Glowinkowski, S.; Ediger, M. D. *Macromolecules* **1991**, *24*, 4270.

(9) Adolf, D. B.; Ediger, M. D. *Macromolecules* **1991**, *24*, 5834.

(10) Zorn, R.; Mopsik, F. I.; McKenna, G. B.; Willner, L.; Richter, D. *J. Chem. Phys.* **1997**, *107*, 3645.

MA002206Q